

A sparse grid discrete ordinate discontinuous Galerkin method for the radiative transfer equation

Jianguo Huang*, Yue Yu

*School of Mathematical Sciences, and MOE-LSC, Shanghai Jiao Tong University
Shanghai 200240, China*

Abstract

The radiative transfer equation is a fundamental equation in transport theory and applications, which is a 5-dimensional PDE in the stationary one-velocity case, leading to great difficulties in numerical simulation. To tackle this bottleneck, we first use the discrete ordinate technique to discretize the scattering term, an integral with respect to the angular variables, resulting in a semi-discrete hyperbolic system. Then, we make the spatial discretization by means of the discontinuous Galerkin (DG) method combined with the sparse grid method. The final linear system is solved by the block Gauss-Seidal iteration method. The computational complexity and error analysis are developed in detail, which show the new method is more efficient than the original discrete ordinate DG method. A series of numerical results are performed to validate the convergence behavior and effectiveness of the proposed method.

Keywords: Radiative transfer equation, Sparse grid method, Discrete ordinate method, Discontinuous Galerkin method

1. Introduction

Radiation transport is a physical process of energy transfer in the form of electromagnetic radiation which is affected by absorption, emission and scattering as it passes through the background materials. The radiative transfer equation (RTE) is an important mathematical model used to describe these interactions, finds applications in a wide variety of subjects, including neutron transport, heat transfer, optics, astrophysics, inertial confinement fusion, and high temperature flow systems, see for examples [2, 12, 16, 20, 27, 40].

The RTE can be viewed as a hyperbolic-type integro-differential equation. Even for the stationary monochromatic RTE, it is five-dimensional in the phase space, and hence cannot have a closed-form solution in general. Thus, the numerical solution of the equation is unavoidable and critical in applications. In history, the Monte-Carlo method is a typical approach for numerical simulation (cf. [11] and the references therein). The advantage

*Corresponding author.

Email addresses: `jghuang@sjtu.edu.cn` (Jianguo Huang), `terenceyuyue@sjtu.edu.cn` (Yue Yu)

is its simplicity and dimension-free convergence, and the weakness is its heavy computational cost and slow convergence. Until now, there have developed many other numerical methods as well. For the angular discretization, the typical methods include discrete ordinate methods (or S_N methods) and spherical harmonic methods (or P_N method); for the spatial discretization, the typical methods include finite difference methods, finite element methods and spectral methods. We refer to [6, 7, 12, 18, 20, 27, 30, 31] for details. Due to the flexibility and easy implementation, the discrete ordinate method is frequently used for angular discretization in practice. If the spatial domain is regular, this semi-discrete method is further discretized by the Chebyshev spectral method in [5, 17, 28] and the meshless discretization in [29, 34, 42]. In recent years, the positivity-preserving schemes are also developed very technically in [15, 45, 47]. For numerical solvers such as source iteration and multigrid algorithms, one can refer to [1, 13, 36, 38].

On the other hand, except the Monte-Carlo method, all the methods mentioned above solve the problems with reduced dimensions. In this paper, we intend to attack the problem in its original form with 3-spatial variables and 2-angular variables. In this case, most usual methods suffer from the so-called “the curse of dimension”, which indicates the low rate of convergence in terms of number of degrees of freedom due to the high dimensionality of the underlying problem. To the best of our knowledge, the sparse grid method, also called the sparse tensor product method, is an effective way to overcome the bottleneck. Historically, the idea of sparse grids can be traced back to Smoljak’s construction of multivariate quadrature formulas using combinations of tensor products of suitable one-dimensional formulas (cf. [19, 39]). More recently, the systematic and thorough studies on the method can be found in [19, 22, 23, 46]. In addition, several sparse grid methods are devised in [21, 44] for solving the RTE through conforming spatial discretization. However, according to the computational experience, it is preferable to use the discontinuous Galerkin (DG) method for spatial discretization for hyperbolic problems (cf. [9, 10, 14]), in order to capture non-smooth physical solutions. In [43], the sparse grid technique combined with the DG method has been developed for elliptic equations. This method is also applied to transport equations in [24, 25], but the scattering effect is not considered. The adaptive analogues of their methods are also given in [25, 41].

In this paper, we are intended to propose and analyze a sparse grid DG method to solve the RTE, following the ideas in [27] and [24]. Unlike the studies in [21, 44], the DG method will be used to carry out the spatial discretization. And different from [24], we will discuss in detail the efficient solution of the 5-dimensional RTE with scattering effect. Concretely speaking, the discrete ordinate technique is first applied to discretize the scattering term, an integral with respect to the angular variables, by simply picking several directions spanning the solid angle, resulting in a semi-discrete coupled hyperbolic system. In view of the hyperbolic nature of the semi-discrete system, the DG method is further employed for spatial discretization, yielding a fully discrete method. To overcome the curse of dimension, the sparse DG space is constructed by using the techniques in wavelet analysis to replace the original piecewise polynomial approximation space. We achieve the complexity analysis and error analysis of the method using some arguments in [27] and [24], which show the new approach can greatly reduce the spatial degrees of freedom while keeping almost

the same accuracy up to multiplication of an log factor. For the resulting linear system, considering its block structure, we solve it using the block Gauss-Seidal iteration method. A series of numerical examples are reported to validate the accuracy and performance of the proposed method. Furthermore, we also extend the method to solve the RTE efficiently for some non-tensor product spatial domains in two dimensions.

We end this section by introducing some notations and symbols frequently used in this paper. For a bounded Lipschitz domain D , the symbol $(\cdot, \cdot)_D$ denotes the L^2 -inner product on D , $\|\cdot\|_{0,D}$ denotes the L^2 -norm, and $|\cdot|_{s,D}$ is the $H^s(D)$ -seminorm. For all integer $k \geq 0$, $\mathbb{P}_k(D)$ is the set of polynomials of degree $\leq k$ on D .

The jumps and averages for scalar and vector-valued functions ($v, \boldsymbol{\tau}$, respectively) on an edge e common to two elements K_1, K_2 are defined by

$$\begin{aligned} \llbracket v \rrbracket &= v_1 \mathbf{n}_1 + v_2 \mathbf{n}_2, & \{\!\!\{ v \}\!\!\} &= \frac{v_1 + v_2}{2}, \\ \llbracket \boldsymbol{\tau} \rrbracket &= \boldsymbol{\tau}_1 \cdot \mathbf{n}_1 + \boldsymbol{\tau}_2 \cdot \mathbf{n}_2, & \{\!\!\{ \boldsymbol{\tau} \}\!\!\} &= \frac{\boldsymbol{\tau}_1 + \boldsymbol{\tau}_2}{2}, \end{aligned}$$

where $\mathbf{n}_1, \mathbf{n}_2$ are the unit outward normals to K_1, K_2 , respectively. On a boundary edge or face, $\llbracket v \rrbracket = v \mathbf{n}$ and $\{\!\!\{ \boldsymbol{\tau} \}\!\!\} = \boldsymbol{\tau}$. Moreover, for any two quantities a and b , “ $a \lesssim b$ ” indicates “ $a \leq Cb$ ” with the hidden constant C independent of the mesh size h_K , and “ $a \approx b$ ” abbreviates “ $a \lesssim b \lesssim a$ ”.

2. Radiative transfer equation

The steady-state monoenergetic version of the radiative transfer equation is expressed as (cf. [6, 27])

$$\boldsymbol{\omega} \cdot \nabla u(\mathbf{x}, \boldsymbol{\omega}) + \sigma_t(\mathbf{x})u(\mathbf{x}, \boldsymbol{\omega}) = \sigma_s(\mathbf{x})(Su)(\mathbf{x}, \boldsymbol{\omega}) + f(\mathbf{x}, \boldsymbol{\omega}), \quad \mathbf{x} \in D, \boldsymbol{\omega} \in S^2. \quad (2.1)$$

Here, D is a domain in \mathbb{R}^3 and S^2 denotes the unit sphere in \mathbb{R}^3 , $u(\mathbf{x}, \boldsymbol{\omega})$ is a function of three space variables \mathbf{x} and two angular variables $\boldsymbol{\omega}$, $\sigma_t = \sigma_a + \sigma_s$ with σ_a being the macroscopic absorption cross section, and σ_s the macroscopic scattering cross section, and f is a source function in D . We impose an inflow boundary value condition

$$u(\mathbf{x}, \boldsymbol{\omega}) = \alpha(\mathbf{x}, \boldsymbol{\omega}), \quad (\mathbf{x}, \boldsymbol{\omega}) \in \Gamma_-, \quad (2.2)$$

where Γ_- is defined by

$$\Gamma_- = \{(\mathbf{x}, \boldsymbol{\omega}) : \mathbf{x} \in \partial D, \boldsymbol{\omega} \in S^2, \mathbf{n}(\mathbf{x}) \cdot \boldsymbol{\omega} < 0\}. \quad (2.3)$$

The symbol S on the right-hand side of (2.1) is an integral operator defined by

$$(Su)(\mathbf{x}, \boldsymbol{\omega}) = \int_{S^2} g(\mathbf{x}, \boldsymbol{\omega} \cdot \hat{\boldsymbol{\omega}})u(\mathbf{x}, \hat{\boldsymbol{\omega}})d\sigma(\hat{\boldsymbol{\omega}}) \quad (2.4)$$

with g being a nonnegative normalized phase function

$$\int_{S^2} g(\mathbf{x}, \boldsymbol{\omega} \cdot \hat{\boldsymbol{\omega}}) d\sigma(\hat{\boldsymbol{\omega}}) = 1, \quad \mathbf{x} \in D, \boldsymbol{\omega} \in S^2.$$

In most applications, the function g is assumed to be independent of \mathbf{x} . One well-known example considered in this paper is the Henyey-Greenstein phase function

$$g(t) = \frac{1 - \eta^2}{4\pi(1 + \eta^2 - 2\eta t)^{3/2}}, \quad t \in [-1, 1], \quad (2.5)$$

where the parameter $\eta \in (-1, 1)$ is the anisotropy factor for the scattering medium which measures the strength of forward peakedness of the phase function. Note that $\eta = 0$ for isotropic scattering, $\eta > 0$ for forward scattering, and $\eta < 0$ for backward scattering.

We assume that

- $\sigma_t, \sigma_s \in L^\infty(D)$, $\sigma_s \geq 0$ a.e. in D , $\sigma_a = \sigma_t - \sigma_s \geq c_0$ in D for a constant $c_0 > 0$.
- $f(\mathbf{x}, \boldsymbol{\omega}) \in L^2(D \times S^2)$ and is a continuous function with respect to $\boldsymbol{\omega} \in S^2$.

Under these assumptions, the problem (2.1)-(2.2) has a unique solution $u \in H_2^1(D \times S^2)$ (cf. [27]), where

$$H_2^1(D \times S^2) := \{v \in L^2(D \times S^2) : \boldsymbol{\omega} \cdot \nabla v \in L^2(D \times S^2)\}.$$

3. The sparse grid discrete-ordinate DG method for the RTE

In this section, we first recall the construction of sparse discontinuous finite element spaces; One can refer to [3, 4, 43] and the references therein for details. Then, we will present in detail the sparse grid discrete-ordinate DG method for the RTE.

3.1. Construction of sparse DG spaces

Let $\Omega = [0, 1]$ and partition it into 2^n cells with uniform cell size $h = 2^{-n}$. The resulting n -th level grid is denoted by Ω_n and the j -th cell is given by

$$I_n^j = (2^{-n}j, 2^{-n}(j+1)], \quad j = 0, 1, \dots, 2^n - 1.$$

We define

$$V_n^k = \{v : v|_{I_n^j} \in \mathbb{P}_k(I_n^j), \quad j = 0, 1, \dots, 2^n - 1\}$$

to be the piecewise polynomial space on Ω_n . One can check that there exists the nested structure for different values of n : $V_0^k \subset V_1^k \subset \dots \subset V_n^k \subset \dots$. Denote W_n^k to be the orthogonal complement of V_{n-1}^k in V_n^k with respect to the $L^2(\Omega)$ inner product, i.e.,

$$V_{n-1}^k \oplus W_n^k = V_n^k, \quad W_n^k \perp V_{n-1}^k, \quad n \geq 1,$$

where for simplicity set $W_0^k = V_0^k$. We then obtain an orthogonal decomposition of the DG space

$$V_N^k = \bigoplus_{0 \leq n \leq N} W_n^k.$$

We proceed to review the construction in multi-dimensions. For $\Omega = [0, 1]^d$, let $h_m = 2^{-n_m}$ be the step size along x_m -direction. For simplicity, we use the notations of multi-indices in the following. Let $\mathbf{n} = (n_1, n_2, \dots, n_d)$. Then the cell size can be denoted by

$$h_{\mathbf{n}} = (2^{-n_1}, 2^{-n_2}, \dots, 2^{-n_d}) = 2^{-\mathbf{n}}$$

and the associated grid is written by $\Omega_{\mathbf{n}}$ whose \mathbf{j} -th cell is given by

$$I_{\mathbf{n}}^{\mathbf{j}} = I_{n_1}^{j_1} \times I_{n_2}^{j_2} \times \dots \times I_{n_d}^{j_d}, \quad \mathbf{j} = (j_1, j_2, \dots, j_d),$$

where

$$I_{n_m}^{j_m} = (2^{-n_m} j_m, 2^{-n_m} (j_m + 1)], \quad j_m = 0, 1, \dots, 2^{n_m} - 1$$

is the element along x_m -axis. With multi-indices notation we have $\mathbf{0} \leq \mathbf{j} \leq 2^{\mathbf{n}} - \mathbf{1}$. Introduce a tensor-product piecewise polynomial space as

$$\mathbf{V}_{\mathbf{n}}^k = \{\mathbf{v} : \mathbf{v}(\mathbf{x}) \in \mathbb{Q}_k(I_{\mathbf{n}}^{\mathbf{j}}), \quad \mathbf{0} \leq \mathbf{j} \leq 2^{\mathbf{n}} - \mathbf{1}\},$$

where $\mathbb{Q}_k(I_{\mathbf{n}}^{\mathbf{j}})$ consists of polynomials of degree up to k in each dimension on cell $I_{\mathbf{n}}^{\mathbf{j}}$. If we use an equal refinement of size $h := h_N = 2^{-N}$ in each coordinate direction, the grid and space will be denoted by Ω_N and \mathbf{V}_N^k , respectively. With the usual convention, we also use \mathcal{T}_h and V_h^k instead.

It is obvious that

$$\mathbf{V}_{\mathbf{n}}^k = V_{n_1}^k \times V_{n_2}^k \times \dots \times V_{n_d}^k.$$

We similarly define the tensor-product multiwavelet space as

$$\mathbf{W}_{\mathbf{n}}^k = W_{n_1}^k \times W_{n_2}^k \times \dots \times W_{n_d}^k.$$

Observing the fact that

$$V_{n_m}^k = \bigoplus_{0 \leq j_m \leq n_m} W_{j_m}^k,$$

we have the following expansion

$$\mathbf{V}_{\mathbf{n}}^k = \bigoplus_{\mathbf{0} \leq \mathbf{j} \leq \mathbf{n}} \mathbf{W}_{\mathbf{j}}^k, \quad \mathbf{V}_N^k = \bigoplus_{|\mathbf{j}|_{\infty} \leq N} \mathbf{W}_{\mathbf{j}}^k.$$

The sparse finite element approximation space on Ω_N is defined by the following truncated space

$$\widehat{\mathbf{V}}_N^k := \bigoplus_{|\mathbf{n}|_1 \leq N} \mathbf{W}_{\mathbf{n}}^k, \quad |\mathbf{n}|_1 = n_1 + n_2 + \dots + n_d.$$

The number of degrees of freedom of sparse DG space is $\mathcal{O}(h^{-1} |\log_2 h|^{d-1})$ with $h = 2^{-N}$, which is significantly less than that of DG space with exponential dependence on d .

3.2. The sparse grid discrete-ordinate DG method

For any continuous function $F(\boldsymbol{\omega})$ defined on the unit sphere S^2 , we write the numerical quadrature to be used in the form

$$\int_{S^2} F(\boldsymbol{\omega}) d\sigma(\boldsymbol{\omega}) \approx \sum_{l=1}^L w_l F(\boldsymbol{\omega}^l), \quad \boldsymbol{\omega}^l \in S^2, \quad 1 \leq l \leq L. \quad (3.1)$$

The integral operator S is then approximated by

$$(Su)(\mathbf{x}, \boldsymbol{\omega}) \approx (S_d u)(\mathbf{x}, \boldsymbol{\omega}) := \sum_{l=1}^L w_l g(\mathbf{x}, \boldsymbol{\omega} \cdot \boldsymbol{\omega}^l) u(\mathbf{x}, \boldsymbol{\omega}^l). \quad (3.2)$$

Regarding the accuracy of the quadrature (3.1), we will write n for the algebraic precision, i.e., the quadrature integrates exactly all spherical polynomials of total degree no more than n and does not integrate exactly some spherical polynomial of total degree $n + 1$. Then we have the following estimate (cf. [27])

$$\left| \int_{S^2} F(\boldsymbol{\omega}) d\sigma(\boldsymbol{\omega}) - \sum_{l=1}^L w_l F(\boldsymbol{\omega}^l) \right| \leq c_s n^{-s} \|F\|_{s, S^2}, \quad F \in H^s(S^2), \quad s > 1, \quad (3.3)$$

where c_s is a universal constant depending only on s . Associated with the numerical quadrature, we further define

$$m(\mathbf{x}) = \max_{1 \leq i \leq L} \sum_{l=1}^L w_l g(\mathbf{x}, \boldsymbol{\omega}^l \cdot \boldsymbol{\omega}^i) \quad (3.4)$$

and make the following assumption (cf. [27]):

$$\sigma_t - m\sigma_s \geq c'_0 \text{ in } D \text{ for some constant } c'_0 > 0. \quad (3.5)$$

Using the quadrature (3.2), we can discretize (2.1) in angular direction to get

$$\boldsymbol{\omega}^l \cdot \nabla u^l + \sigma_t u^l = \sigma_s(\mathbf{x}) \sum_{i=1}^L w_i g(\mathbf{x}, \boldsymbol{\omega}^l \cdot \boldsymbol{\omega}^i) u^i + f^l, \quad 1 \leq l \leq L \quad (3.6)$$

with boundary value condition

$$u^l(\mathbf{x}) = \alpha^l(\mathbf{x}), \quad (\mathbf{x}, \boldsymbol{\omega}^l) \in \Gamma_-, \quad 1 \leq l \leq L, \quad (3.7)$$

where $u^l = u^l(\mathbf{x})$ is the approximation to $u(\mathbf{x}, \boldsymbol{\omega}^l)$.

The system (3.6) is a first-order hyperbolic problem in space, which will be further discretized by DG method. Let $\{\mathcal{T}_h\}_{h>0}$ be a regular family of triangulations of D . Assume that \mathcal{E}_h consists of the set of all edges ($d = 2$) or faces ($d = 3$) in \mathcal{T}_h and \mathcal{E}_h^0 the set of all interior edges or faces. By a direct manipulation, we obtain the following identity (cf. [10]):

Lemma 3.1. For $(\varphi, \boldsymbol{\tau}) \in H^s(\mathcal{T}_h) \times [H^s(\mathcal{T}_h)]^d$, $s > 1/2$, there holds

$$\sum_{K \in \mathcal{T}_h} \int_{\partial K} \varphi \boldsymbol{\tau} \cdot \mathbf{n} ds = \sum_{e \in \mathcal{E}_h} \int_e \{\{\boldsymbol{\tau}\}\} \cdot \llbracket \varphi \rrbracket ds + \sum_{e \in \mathcal{E}_h^0} \int_e \{\{\varphi\}\} \cdot \llbracket \boldsymbol{\tau} \rrbracket ds. \quad (3.8)$$

Further, if $u \in H^s(\omega_e)$ and $s > 1/2$, then we have the following weak continuity

$$\int_e \llbracket u \rrbracket v ds = 0, \quad v \in L^2(e), \quad e \in \mathcal{E}_h^0,$$

where ω_e is the set of elements sharing e as an edge ($d = 2$) or faces ($d = 3$).

We define a discontinuous finite element space by

$$V_h = \left\{ v \in L^2(D) : v|_K \in \mathbb{P}_k(K), \quad K \in \mathcal{T}_h \right\}, \quad (3.9)$$

where $\mathbb{P}_k(K)$ denotes the set of all polynomials on K with degree $\leq k$. Multiplying (3.6) by any $v_h \in V_h$, we obtain from the integration by parts that

$$\begin{aligned} & \sum_{K \in \mathcal{T}_h} \left[\int_K (-u^l(\boldsymbol{\omega}^l \cdot \nabla v_h) + \sigma_t u^l v_h) dx + \int_{\partial K} (\boldsymbol{\omega}^l \cdot \mathbf{n}) u^l v_h ds \right] \\ &= \int_D \sigma_s \sum_{i=1}^L w_i g(\cdot, \boldsymbol{\omega}^i) u^i v_h dx + \int_D f^l v_h dx, \quad 1 \leq l \leq L. \end{aligned}$$

Taking $\boldsymbol{\tau} = \boldsymbol{\omega}^l u^l$ and $\varphi = v_h$ in (3.8), we immediately obtain the following system

$$a_h^{(l)}(u^l, v_h) + b_h^{(l)}(u^l, v_h) = (f^l, v_h) + \langle \alpha^l, v_h \rangle^{(l)}, \quad v_h \in V_h,$$

where

$$\begin{aligned} a_h^{(l)}(u^l, v_h) &= \sum_{K \in \mathcal{T}_h} \int_K (-u^l(\boldsymbol{\omega}^l \cdot \nabla v_h) + \sigma_t u^l v_h) dx \\ &\quad - \int_D \sigma_s \sum_{i=1}^L w_i g(\cdot, \boldsymbol{\omega}^i) u^i v_h dx, \end{aligned} \quad (3.10)$$

$$b_h^{(l)}(u^l, v_h) = \sum_{e \in \Gamma_-} \int_e \{\{\boldsymbol{\omega}^l u^l\}\} \cdot \llbracket v_h \rrbracket ds, \quad (3.11)$$

$$(f^l, v_h) = \int_D f^l v_h dx, \quad \langle \alpha^l, v_h \rangle^{(l)} = - \sum_{e \in \Gamma_-} \int_e \boldsymbol{\omega}^l \cdot \mathbf{n} \alpha^l v_h ds. \quad (3.12)$$

Define $\mathbf{V}_h = (V_h)^L$ and write a generic element as $\mathbf{v}_h := \{v_h^l\}_{l=1}^L$. The global formulation can be expressed as

$$\sum_{l=1}^L w_l (a_h^{(l)}(u^l, v_h^l) + b_h^{(l)}(u^l, v_h^l)) = \sum_{l=1}^L w_l ((f^l, v_h^l) + \langle \alpha^l, v_h^l \rangle^{(l)}).$$

Then the discrete-ordinate DG method is: Find $\mathbf{u}_h := \{u_h^l\} \in \mathbf{V}_h$ such that

$$a_h(\mathbf{u}_h, \mathbf{v}_h) = F(\mathbf{v}_h), \quad \mathbf{v}_h \in \mathbf{V}_h, \quad (3.13)$$

where

$$\begin{aligned} a_h(\mathbf{u}_h, \mathbf{v}_h) &= \sum_{l=1}^L w_l (a_h^{(l)}(u_h^l, v_h^l) + b_h^{(l)}(u_h^l, v_h^l)), \\ F(\mathbf{v}_h) &= \sum_{l=1}^L w_l ((f^l, v_h^l) + \langle \alpha^l, v_h^l \rangle^{(l)}). \end{aligned}$$

It is preferable to add some stabilization terms in the DG scheme to penalize the jump of the solution across interior edges or faces of the triangulation. One approach introduced in [10] is to replace the average $\{\{\boldsymbol{\omega}^l u^l\}\}$ in (3.11) by $\{\{\boldsymbol{\omega}^l u_h^l\}\} + c_e^l \llbracket u_h^l \rrbracket$, where c_e^l is a nonnegative function over e satisfying $c_e^l = \theta_0 |\boldsymbol{\omega}^l \cdot \mathbf{n}|$ with θ_0 a constant independent of e and h . The stabilized discrete-ordinate DG method is to find $\mathbf{u}_h := \{u_h^l\} \in \mathbf{V}_h$ such that

$$a_h^s(\mathbf{u}_h, \mathbf{v}_h) = F(\mathbf{v}_h), \quad \mathbf{v}_h \in \mathbf{V}_h, \quad (3.14)$$

where

$$a_h^s(\mathbf{u}_h, \mathbf{v}_h) = \sum_{l=1}^L w_l (a_h^{(l)}(u_h^l, v_h^l) + b_{hs}^{(l)}(u_h^l, v_h^l)) \quad (3.15)$$

and

$$\begin{aligned} b_{hs}^{(l)}(u_h^l, v_h^l) &= b_h^{(l)}(u_h^l, v_h^l) + \sum_{e \in \mathcal{E}_h^0} \int_e c_e^l \llbracket u_h^l \rrbracket \cdot \llbracket v_h^l \rrbracket ds \\ &= \sum_{e \notin \Gamma_-} \int_e \{\{\boldsymbol{\omega}^l u_h^l\}\} \cdot \llbracket v_h^l \rrbracket ds + \sum_{e \in \mathcal{E}_h^0} \int_e c_e^l \llbracket u_h^l \rrbracket \cdot \llbracket v_h^l \rrbracket ds. \end{aligned} \quad (3.16)$$

Remark 3.1. The sparse grid discrete-ordinate DG method is obtained by replacing the DG space V_h in (3.9) with the sparse DG space $\widehat{V}_h^k := \widehat{\mathbf{V}}_N^k \subset V_h$.

4. Error analysis

4.1. Error estimate of the sparse projection operator

We define the broken H^s Sobolev norm on Ω_N by

$$\|v\|_{H^s(\Omega_N)}^2 = \sum_{\mathbf{0} \leq \mathbf{j} \leq \mathbf{2}^{\mathbf{N}-1}} \|v\|_{H^s(I_N^{\mathbf{j}})}^2.$$

For any nonnegative integer m and the multi-index $\alpha = \{i_1, i_2, \dots, i_r\} \subset \{1, 2, \dots, d\}$, define

$$|v|_{H^{m,\alpha}(\Omega)} = \left\| \left(\frac{\partial^m}{\partial x_{i_1}^m} \cdots \frac{\partial^m}{\partial x_{i_r}^m} \right) v \right\|_{L^2(\Omega)}$$

and

$$|v|_{\mathcal{H}^{q+1}(\Omega)} = \max_{1 \leq r \leq d} \left(\max_{\alpha \in \{1, 2, \dots, d\}, |\alpha|=r} |v|_{H^{q+1, \alpha}(\Omega)} \right),$$

which is the norm for the mixed derivative of v of at most degree $q + 1$ in each direction.

In the following, we denote by \mathbf{P} the sparse projection operator to be the L^2 projection onto $\widehat{\mathbf{V}}_N^k$.

Lemma 4.1. *Let \mathbf{P} be the sparse projector, $k \geq 1$, $N \geq 1$ and $d \geq 2$. Then for $v \in \mathcal{H}^{p+1}(\Omega)$ there hold*

$$|\mathbf{P}v - v|_{L^2(\Omega_N)} \lesssim |\log_2 h|^d h^{k+1} |v|_{\mathcal{H}^{k+1}(\Omega)},$$

$$|\mathbf{P}v - v|_{H^1(\Omega_N)} \lesssim h^k |v|_{\mathcal{H}^{k+1}(\Omega)},$$

and

$$\left(\sum_{K \in \mathcal{T}_h} \|\mathbf{P}v - v\|_{0, \partial K}^2 \right)^{1/2} \lesssim |\log_2 h|^d h^{k+1/2} |v|_{\mathcal{H}^{k+1}(\Omega)}.$$

Proof. It follows from [24, 35, 43] that for any $v \in \mathcal{H}^{p+1}(\Omega)$ and $1 \leq q \leq \min\{p, k\}$, there holds

$$|\mathbf{P}v - v|_{H^s(\Omega_N)} \lesssim \begin{cases} N^d 2^{-N(q+1)} |v|_{\mathcal{H}^{q+1}(\Omega)}, & s = 0, \\ 2^{-Nq} |v|_{\mathcal{H}^{q+1}(\Omega)}, & s = 1. \end{cases}$$

Noting that $h = h_N = 2^{-N}$, we have

$$|\mathbf{P}v - v|_{L^2(\Omega_N)} \lesssim |\log_2 h|^d h^{k+1} |v|_{\mathcal{H}^{k+1}(\Omega)}$$

and

$$|\mathbf{P}v - v|_{H^1(\Omega_N)} \lesssim h^k |v|_{\mathcal{H}^{k+1}(\Omega)}.$$

Recalling the trace inequality (cf. [8])

$$\|\phi\|_{0, \partial K}^2 \lesssim h_K^{-1} \|\phi\|_{0, K}^2 + h_K |\phi|_{1, K}^2, \quad (4.1)$$

where $K \in \mathcal{T}_h$ with diameter h_K , we then have

$$\begin{aligned} \left(\sum_{K \in \mathcal{T}_h} \|\mathbf{P}v - v\|_{0, \partial K}^2 \right)^{1/2} &\lesssim \left(\sum_{K \in \mathcal{T}_h} h_K^{-1} \|\mathbf{P}v - v\|_{0, K}^2 + h_K |\mathbf{P}v - v|_{1, K}^2 \right)^{1/2} \\ &\lesssim (|\log_2 h|^{2d} + 1)^{1/2} h^{k+1/2} |v|_{\mathcal{H}^{k+1}(\Omega)} \\ &\lesssim |\log_2 h|^d h^{k+1/2} |v|_{\mathcal{H}^{k+1}(\Omega)}. \end{aligned}$$

This completes the proof. □

4.2. Error analysis of the sparse grid discrete-ordinate DG method

Using the similar arguments in [10, 27], one can deduce the following stability result whose proof is omitted for simplicity.

Lemma 4.2. *Let*

$$\|\mathbf{v}_h\| = \left[\sum_{l=1}^L w_l \left(\sum_{e \in \mathcal{E}_h} c_e^l \|v_h^l\|^2 ds + \int_D (v_h^l)^2 dx \right) \right]^{1/2}.$$

Under the assumption (3.5), there holds

$$a_h^s(\mathbf{v}_h, \mathbf{v}_h) \gtrsim \|\mathbf{v}_h\|^2, \quad \mathbf{v}_h \in \mathbf{V}_h.$$

We denote the solutions of the original problem (2.1), the semi-discrete problem (3.6) and the stabilized discrete-ordinate DG method (3.14) by $\{u(\mathbf{x}, \boldsymbol{\omega}^l)\}$, $\mathbf{u} = \{u^l(\mathbf{x})\}$ and $\mathbf{u}_h = \{u_h^l\}$, respectively. The error is decomposed as

$$\{u(\mathbf{x}, \boldsymbol{\omega}^l)\} - \mathbf{u}_h = (\{u(\mathbf{x}, \boldsymbol{\omega}^l)\} - \{u^l(\mathbf{x})\}) + (\{u^l(\mathbf{x})\} - \{u_h^l(\mathbf{x})\}), \quad (4.2)$$

and measured by

$$\|u - u_h\|_h = \left(\sum_{l=1}^L w_l \|u(\cdot, \boldsymbol{\omega}^l) - u_h^l\|_{0,D}^2 \right)^{1/2}. \quad (4.3)$$

Theorem 4.1. *Let n be the degree of precision of the numerical quadrature and $d \geq 2$. Then under the assumption (3.5), for the sparse grid discrete-ordinate DG method, we have*

$$\begin{aligned} \|u - u_h\|_h &\lesssim c(\theta_0) |\log_2 h|^{d+1} h^{k+1/2} \left(\sum_{l=1}^L w_l |u^l|_{\mathcal{H}^{k+1}(\Omega)}^2 \right)^{1/2} \\ &\quad + c(r', g) n^{-r'} \left(\int_D \|u(\mathbf{x}, \cdot)\|_{r', S^2}^2 dx \right)^{1/2}, \end{aligned}$$

where, $h = 2^{-N}$, u^l is the solution of (3.6), $c(\theta_0) = \theta_0^{-1/2} + \theta_0^{1/2}$ and $c(r', g)$ is defined in (4.4).

Proof. For the first part in (4.2), let

$$\varepsilon^l(\mathbf{x}) := u(\mathbf{x}, \boldsymbol{\omega}^l) - u^l(\mathbf{x}), \quad 1 \leq l \leq L.$$

In view of the equation (4.19) in [27], one has

$$\sum_{l=1}^L w_l \int_D (\varepsilon^l)^2 dx \lesssim c(r', g)^2 n^{-2r'} \int_D \|u(\mathbf{x}, \cdot)\|_{r', S^2}^2 dx,$$

where

$$c(r', g) := c(r') \sup_{\mathbf{x} \in D, \boldsymbol{\omega} \in S^2} \|g(\mathbf{x}, \boldsymbol{\omega} \cdot)\|_{r', S^2} \quad (4.4)$$

and $c(r')$ is a positive constant depending only on r' .

For the second part, let

$$u^l - u_h^l = (u^l - P_h^k u^l) - (u_h^l - P_h^k u^l) =: \eta^l + \delta^l,$$

where P_h^k is the L^2 -projection onto the sparse DG space \widehat{V}_h^k (cf. Remark 3.1). Similarly, we denote $\boldsymbol{\eta} = \{\eta^l\}$ and $\boldsymbol{\delta} = \{\delta^l\}$. When \mathbf{u}_h is replaced by the exact solution \mathbf{u} of the semi-discrete problem, the weak continuity in Lemma 3.1 yields

$$\int_e c_e^l \llbracket u^l \rrbracket \llbracket v_h^l \rrbracket ds = 0, \quad e \in \mathcal{E}_h^0.$$

From (3.16) we have $b_{hs}^{(l)}(u^l, v_h^l) = b_h^{(l)}(u^l, v_h^l)$, and hence $a_h^s(\mathbf{u}, \mathbf{v}_h) = a_h(\mathbf{u}, \mathbf{v}_h)$, which yields the following Galerkin orthogonality

$$a_h^s(\mathbf{u} - \mathbf{u}_h, \mathbf{v}_h) = a_h(\mathbf{u} - \mathbf{u}_h, \mathbf{v}_h) = 0, \quad \mathbf{v}_h \in \mathbf{V}_h. \quad (4.5)$$

According to the stability estimate in Lemma 4.2, we have

$$\|\boldsymbol{\delta}\|^2 \lesssim a_h^s(\boldsymbol{\delta}, \boldsymbol{\delta}) = a_h^s(\mathbf{u}_h - P_h^k \mathbf{u}, \boldsymbol{\delta}) = a_h^s(\mathbf{u} - P_h^k \mathbf{u}, \boldsymbol{\delta}) = a_h^s(\boldsymbol{\eta}, \boldsymbol{\delta}). \quad (4.6)$$

We now estimate the right-hand side of (4.6). Let

$$a_h^{(l)}(u^l, v_h) = \mathbb{I}_1^l(u^l, v_h) - \mathbb{I}_2^l(u^l, v_h),$$

where

$$\begin{aligned} \mathbb{I}_1^l(u^l, v_h) &= \sum_{K \in \mathcal{T}_h} \int_K (-u^l(\boldsymbol{\omega}^l \cdot \nabla v_h) + \sigma_t u^l v_h) dx, \\ \mathbb{I}_2^l(u^l, v_h) &= \int_D \sigma_s \sum_{i=1}^L w_i g(\cdot, \boldsymbol{\omega}^l \cdot \boldsymbol{\omega}^i) u^l v_h dx. \end{aligned}$$

For the first term \mathbb{I}_1^l , noting that $\boldsymbol{\omega}^l \cdot \nabla \delta^l|_K \in \mathbb{Q}_k(K)$, by the definition of the projector P_h^k ,

$$\int_K \eta^l(\boldsymbol{\omega}^l \cdot \nabla \delta^l) dx = \int_K (u^l - P_h^k u^l)(\boldsymbol{\omega}^l \cdot \nabla \delta^l) dx = 0,$$

which gives

$$|\mathbb{I}_1^l(\eta^l, \delta^l)| = \left| \sum_{K \in \mathcal{T}_h} \int_K (-\eta^l(\boldsymbol{\omega}^l \cdot \nabla \delta^l) + \sigma_t \eta^l \delta^l) dx \right| \lesssim \sum_{K \in \mathcal{T}_h} \|\eta^l\|_{0,K} \|\delta^l\|_{0,K}.$$

The Cauchy-Schwarz inequality yields

$$\left| \sum_{l=1}^L w_l \mathbb{I}_1^l(\eta^l, \delta^l) \right| = \left(\sum_{l=1}^L w_l \|\eta^l\|_{0,D}^2 \right)^{1/2} \left(\sum_{l=1}^L w_l \|\delta^l\|_{0,D}^2 \right)^{1/2}.$$

For the second one, using Lemma 4.3 in [27], we obtain

$$\begin{aligned} \left| \sum_{l=1}^L w_l \mathbb{I}_2^l(\eta^l, \delta^l) \right| &\leq \left(\sum_{l=1}^L w_l \int_D m \sigma_s(\eta^l)^2 dx \right)^{1/2} \left(\sum_{l=1}^L w_l \int_D m \sigma_s(\delta^l)^2 dx \right)^{1/2} \\ &\lesssim \left(\sum_{l=1}^L w_l \|\eta^l\|_{0,D}^2 \right)^{1/2} \left(\sum_{l=1}^L w_l \|\delta^l\|_{0,D}^2 \right)^{1/2}, \end{aligned}$$

where $m = m(\mathbf{x})$ is given in (3.4).

It remains to consider $b_{hs}^{(l)}(\eta^l, \delta^l)$. From (49) in [10] we have

$$|b_{hs}^{(l)}(\eta^l, \delta^l)| \leq \sum_{e \in \mathcal{E}_h} \left(\frac{1}{\theta_0} \|c_e^{1/2} \{\eta^l\}\|_{0,e} + \|c_e^{1/2} [\eta^l]\|_{0,e} \right) \|c_e^{1/2} [\delta^l]\|_{0,e}.$$

According to the choice of c_e^l , the Cauchy-Schwarz inequality gives

$$\left| \sum_{l=1}^L w_l b_{hs}^{(l)}(\eta^l, \delta^l) \right| \lesssim c(\theta_0) \left(\sum_{l=1}^L w_l \sum_{K \in \mathcal{T}_h} \|\eta^l\|_{0,\partial K}^2 \right)^{1/2} \left(\sum_{l=1}^L w_l \sum_{e \in \mathcal{E}_h} \|c_e^{1/2} [\delta^l]\|_{0,e}^2 \right)^{1/2},$$

where $c(\theta_0) = \theta_0^{-1/2} + \theta_0^{1/2}$ is a constant, and hence

$$a_h^s(\boldsymbol{\eta}, \boldsymbol{\delta}) \lesssim c(\theta_0) \left[\sum_{l=1}^L w_l \left(\|\eta^l\|_{0,D}^2 + \sum_{K \in \mathcal{T}_h} \|\eta^l\|_{0,\partial K}^2 \right) \right]^{1/2} \|\boldsymbol{\delta}\|.$$

This combined with (4.6) yields

$$\|\boldsymbol{\delta}\| \lesssim c(\theta_0) \left[\sum_{l=1}^L w_l \left(\|\eta^l\|_{0,D}^2 + \sum_{K \in \mathcal{T}_h} \|\eta^l\|_{0,\partial K}^2 \right) \right]^{1/2},$$

and with the error estimates of the sparse projection in Lemma 4.1 leads to the desired result. \square

5. Numerical results

In this section, we shall provide a series of numerical examples for solving the RTE (2.1)-(2.2) to illustrate the performance of the proposed sparse grid discrete coordinate DG method.

5.1. The linear system from the discrete problem

The S_n method has $n(n+2)$ directions with n an even natural number. The discrete-ordinate sets satisfying the required moment equations to fourteen digits of accuracy have been given in [7]. Note that only the ordinates in the first octant are given there. The

Tab. 1. Discrete-ordinate sets for S_2 ($\boldsymbol{\omega} = (s_1, s_2, s_3)$)

s_1	s_2	s_3	w
± 0.5773502691896257	± 0.5773502691896257	± 0.5773502691896257	1.5707963267948966

remaining ordinates can be obtained by using symmetry arguments. For example, S_2 data is given in Tab. 1.

Relabel the sparse bases by a single index $i = 1, 2, \dots, M$ and denote them by φ_i , where $M = \dim \widehat{\mathbf{V}}_N^k$. The variational problem (3.14) can be written in matrix form

$$\mathbf{A}^{(l)} \hat{\mathbf{U}}^l - \sum_{i=1}^L \mathbf{B}_i^{(l)} \hat{\mathbf{U}}^i + \mathbf{C}^{(l)} \hat{\mathbf{U}}^l = \mathbf{F}^{(l)}, \quad 1 \leq l \leq L, \quad (5.1)$$

where

$$\begin{aligned} \mathbf{A}^{(l)} &= (a_{nm}^{(l)}), \quad \mathbf{B}_i^{(l)} = (b_{nmi}^{(l)}), \quad \mathbf{C}^{(l)} = (c_{nm}^{(l)}), \\ \hat{\mathbf{U}}^l &= [\hat{u}_1^l, \hat{u}_2^l, \dots, \hat{u}_M^l]^T, \quad \mathbf{F}^{(l)} = [F_1^{(l)}, F_2^{(l)}, \dots, F_M^{(l)}]^T, \end{aligned}$$

and

$$\begin{aligned} a_{nm}^{(l)} &= \sum_{K \in \mathcal{T}_h} \int_K (-\varphi_m(\boldsymbol{\omega}^l \cdot \nabla \varphi_n) + \sigma_t \varphi_m \varphi_n) dx, \\ b_{nmi}^{(l)} &= w_i \int_D \sigma_s g(\cdot, \boldsymbol{\omega}^l \cdot \boldsymbol{\omega}^i) \varphi_m \varphi_n dx, \\ c_{nm}^{(l)} &= \sum_{e \in \Gamma_-} \int_e \{\{\boldsymbol{\omega}^l \varphi_m\}\} \cdot [\varphi_n] ds + \sum_{e \in \mathcal{E}_h^0} \int_e c_e^l [\varphi_m] \cdot [\varphi_n] ds, \\ F_n^{(l)} &= \int_D f^l \varphi_n dx - \sum_{e \in \Gamma_-} \int_e \boldsymbol{\omega}^l \cdot \mathbf{n} \alpha^l \varphi_n ds. \end{aligned}$$

The system (5.1) can be further rewritten in block matrix form

$$\mathbf{D}^{(l)} \hat{\mathbf{U}} = \mathbf{F}^{(l)}, \quad 1 \leq l \leq L,$$

where

$$\mathbf{D}^{(l)} := [-\mathbf{B}_1^{(l)}, \dots, -\mathbf{B}_{l-1}^{(l)}, \mathbf{A}^{(l)} - \mathbf{B}_l^{(l)} + \mathbf{C}^{(l)}, \dots, -\mathbf{B}_L^{(l)}].$$

The final linear system is

$$\mathbf{D} \hat{\mathbf{U}} = \mathbf{F}, \quad (5.2)$$

where

$$\mathbf{D} = \begin{bmatrix} \mathbf{D}^{(1)} \\ \vdots \\ \mathbf{D}^{(L)} \end{bmatrix}, \quad \hat{\mathbf{U}} = \begin{bmatrix} \hat{\mathbf{U}}^1 \\ \vdots \\ \hat{\mathbf{U}}^L \end{bmatrix}, \quad \mathbf{F} = \begin{bmatrix} \mathbf{F}^{(1)} \\ \vdots \\ \mathbf{F}^{(L)} \end{bmatrix}.$$

We solve (5.2) by using the block Gauss-Seidal iteration method.

The accuracy is measured by the weighted relative error defined by

$$\|u - u_h\|_{rel} = \frac{\left(\sum_{l=1}^L \omega_l \|u(\cdot, \boldsymbol{\omega}^l) - u_h^l\|_{0,D}^2 \right)^{1/2}}{\left(\sum_{l=1}^L \omega_l \|u(\cdot, \boldsymbol{\omega}^l)\|_{0,D}^2 \right)^{1/2}},$$

where $u_h^l = \sum_{m=1}^M \hat{u}_m^l \varphi_m$ is the numerical solution.

5.2. Examples in three dimensions

Example 5.1. We take $\sigma_t = 2$, $\sigma_s = 1$ and $\eta = 0$. The domain D is a unit cube. With the right-hand side function

$$f(\mathbf{x}, \boldsymbol{\omega}) = \pi s_1 \cos(\pi x_1) \sin(\pi x_2) \sin(\pi x_3) + \pi s_2 \sin(\pi x_1) \cos(\pi x_2) \sin(\pi x_3) \\ + \pi s_3 \sin(\pi x_1) \sin(\pi x_2) \cos(\pi x_3) + \sin(\pi x_1) \sin(\pi x_2) \sin(\pi x_3),$$

where $\boldsymbol{\omega} = (s_1, s_2, s_3)$, the exact solution is

$$u(\mathbf{x}, \boldsymbol{\omega}) = \sin(\pi x_1) \sin(\pi x_2) \sin(\pi x_3).$$

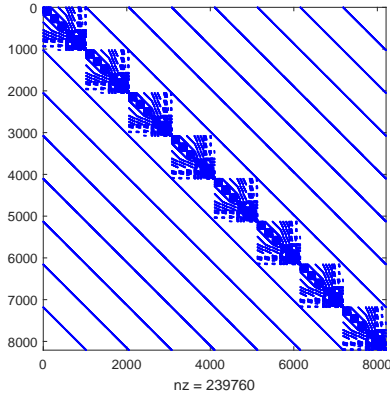


Fig. 1. Sparse pattern of the coefficient matrix for Example 5.1 ($N = 3, k = 2, n = 2$)

The sparse pattern for the coefficient matrix is shown in Fig. 1. The total number of the entries is $8200 \times 8200 = 67371264$ and the number of nonzero elements is $\text{nz} = 239760$. Thus the sparsity ratio is 99.64%.

Fig. 2 displays the expansion coefficients which coincide in each angular direction since the true solution is independent of the angular variable $\boldsymbol{\omega}$. We observe a better result for bigger stabilization parameter θ_0 . In the following we always choose $\theta_0 = 10^{N+k}$ due to its good performance in different cases. For the isotropic case $\eta = 0$, S_2 method is enough to resolve the solution accurately in angle as indicated by the numerical results in Tabs. 2 and

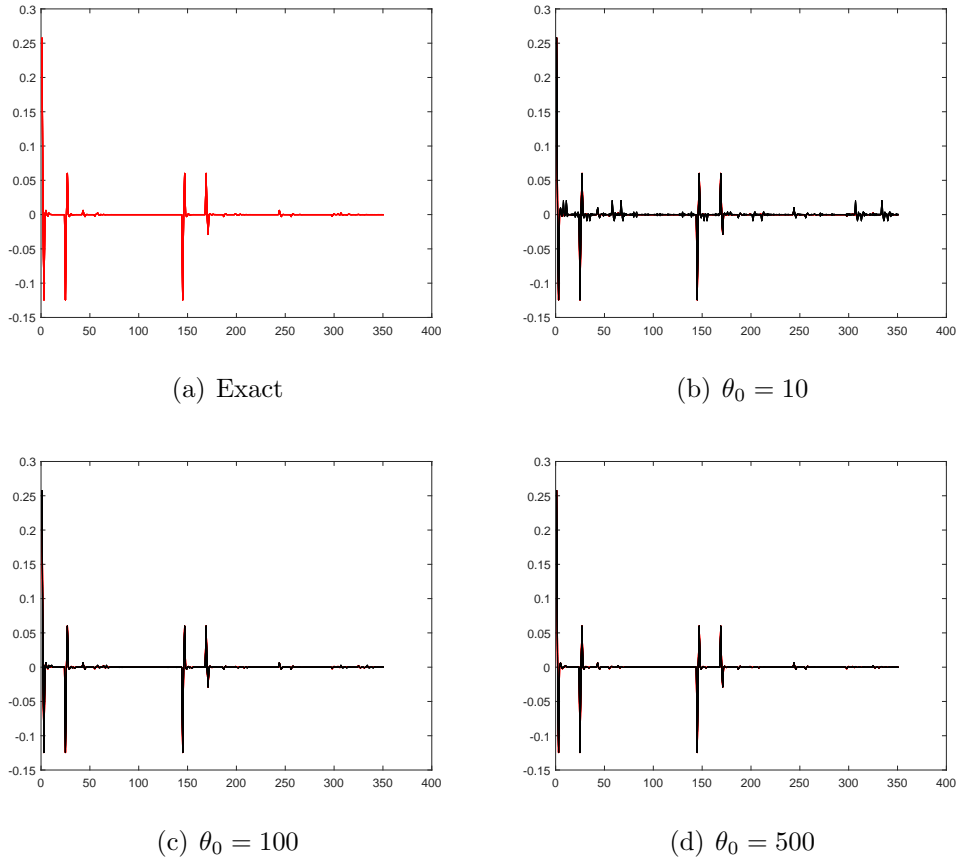


Fig. 2. The expansion coefficients for Example 5.1 with different stabilization parameters ($S_2, k = 2$)

Tab. 2. Relative errors for Example 5.1: k v.s. S_n ($N = 2$)

n	2	4	6	8	10
$k = 1$	1.7133e-01	1.7329e-01	1.7480e-01	1.7491e-01	1.7500e-01
$k = 2$	8.9453e-03	8.3749e-03	8.0365e-03	8.0532e-03	8.0755e-03

Tab. 3. Relative errors for Example 5.1: N v.s. S_n ($k = 2$)

n	2	4	6	8	10
$N = 2$	8.9453e-03	8.3749e-03	8.0365e-03	8.0532e-03	8.0755e-03
$N = 3$	2.2512e-03	2.1269e-03	2.0150e-03	2.0138e-03	2.0136e-03

3. For the given example, the error is then dominated by the spatial problems. According to Theorem 4.1, the error bound is $\mathcal{O}(c(\theta_0)|\log_2 h|^d h^{k+1/2})$. With the choice for θ_0 in this case, we have $c(\theta_0)|\log_2 h|^d h^{k+1/2} \approx \mathcal{O}(|\log_2 h|^d h^k)$ and the logarithmic factor implies a slightly lower order than k . From Tab. 4, we see that the convergence rates for $k = 1, 3$ are better

than $\mathcal{O}(h^{k+1/2})$ and even the $(k + 1)$ -th order can be obtained for $k = 3$. For $k = 2, 4$ the order is about k .

Tab. 4. L^2 errors of S_2 method for Example 5.1

N	$k = 1$		$k = 2$		$k = 3$		$k = 4$	
	Err	rate	Err	rate	Err	rate	Err	rate
1	4.8695e-01	-	3.7626e-02	-	3.8603e-03	-	2.9324e-04	-
2	1.7133e-01	1.5070	8.9453e-03	2.0725	2.1133e-04	4.1911	1.6406e-05	4.1598
3	5.6436e-02	1.6021	2.2512e-03	1.9904	1.2971e-05	4.0261	7.8260e-07	4.3898
4	1.6990e-02	1.7319	5.6295e-04	1.9996	8.2285e-07	3.9785	-	-

Example 5.2. We take $\sigma_t = 3$ and $\sigma_s = 1$. The domain D is a unit cube. The true solution is taken as

$$u(\mathbf{x}, \boldsymbol{\omega}) = 10\omega_3 \sin(\pi x_1) \sin(\pi x_2) \sin(\pi x_3),$$

from which we know after a direct manipulation that the right-hand side function is

$$\begin{aligned} f(\mathbf{x}, \mathbf{s}) = & 10(\sigma_t - \eta\sigma_s)s_3 \sin(\pi x_1) \sin(\pi x_2) \sin(\pi x_3) \\ & + 10\pi s_3^2 \sin(\pi x_1) \sin(\pi x_2) \cos(\pi x_3) + 10\pi s_2 s_3 \sin(\pi x_1) \cos(\pi x_2) \sin(\pi x_3) \\ & + 10\pi s_1 s_3 \cos(\pi x_1) \sin(\pi x_2) \sin(\pi x_3) \end{aligned}$$

where $\boldsymbol{\omega} = (s_1, s_2, s_3)$.

Tab. 5. Relative errors for Example 5.2 ($S_2, \eta = 0.1$)

N	$k = 1$	$k = 2$	$k = 3$	$k = 4$
1	2.2797e-01	1.6584e-02	1.7683e-03	2.1850e-04
2	8.2048e-02	3.7848e-03	2.0045e-04	1.7282e-04

Tab. 6. Relative errors for Example 5.2 ($N = 1, \eta = 0.9$)

n	$k = 1$	$k = 2$	$k = 3$	$k = 4$
2	6.6685e-01	6.6872e-01	6.6969e-01	2.0653e+01
4	6.4693e-01	1.4665e+01	1.5884e+01	1.6226e+01
6	1.1411e+00	1.2068e+00	1.2539e+00	1.2606e+00
8	1.1511e-01	1.3098e-01	1.3206e-01	1.3212e-01
10	7.3980e-02	7.8657e-02	7.9128e-02	7.9144e-02
12	4.3524e-02	3.2606e-02	3.2684e-02	3.2690e-02

We observe from Tab. 5 that S_2 method is accurate enough for the anisotropy factor close to isotropic cases. However, for strong forward scattering of $\eta = 0.9$, it does not give a satisfactory result. We have to choose a larger n to get an improved result, which, however,

is not expected in real applications since S_n method has $n(n+2)$ angular directions and hence $n(n+2)$ coupled spatial problems. In this case, some models have been developed to approximate the integral operator (cf. [26, 37, 48]). Another approach is to combine the sparse grid technique with the spherical harmonic method.

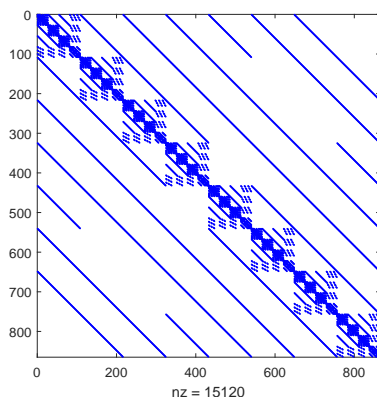


Fig. 3. Sparse pattern of the coefficient matrix for Example 5.3 ($N = 1, k = 2, n = 2$)

Example 5.3. This example is taken from the reference [32], where the Henyey-Greenstein function is replaced by the simplified approximate Mie (SAM):

$$g(t) = K_S(1+t)^{n_p}, \quad t \in [-1, 1],$$

where $n_p = \frac{2\eta}{1-\eta}$ is the anisotropic index and $K_S = \frac{1}{2\pi} \frac{n_p+1}{2^{n_p+1}}$ is the normalization factor. The geometric parameters and the true solution are the same as Example 5.2.

For S_2 method with $N = 1$ and $k = 2$, the sparse pattern for the coefficient matrix is shown in Fig. 3. We also display the numerical and exact coefficients and L^2 projections at $z = 0$ associated with the first angular direction in Fig. 4. We repeat the test for highly forward-peaked scattering with $\eta = 0.9$. From Tab. 7 we observe a relatively smaller errors than that from Tab. 6, but the convergence behaviours are the same since the errors do not decrease significantly with the increase of k and n .

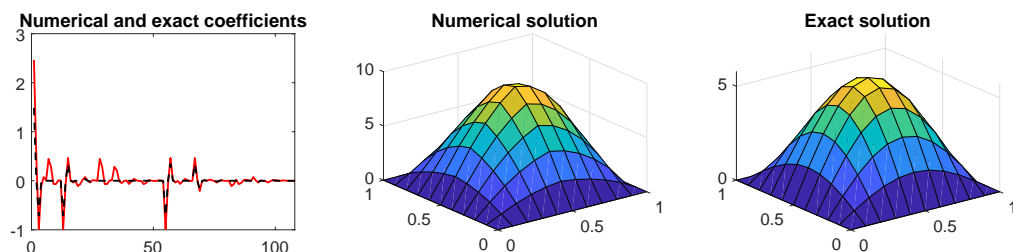


Fig. 4. Numerical and exact coefficients and L^2 projections for Example 5.3 ($N = 1, k = 2, n = 2$)

Tab. 7. Relative errors for Example 5.3 ($N = 1, \eta = 0.9$)

n	$k = 1$	$k = 2$	$k = 3$	$k = 4$
2	6.0818e-01	7.2904e-01	7.3901e-01	7.3967e-01
4	3.7295e-01	4.0517e-02	3.1238e-02	3.1143e-02
6	3.7622e-01	3.7490e-02	2.7350e-02	2.7243e-02
8	3.7823e-01	2.8034e-02	1.0114e-02	9.7213e-03
10	3.7872e-01	2.6477e-02	3.5129e-03	2.0719e-03
12	3.7875e-01	2.6452e-02	3.2775e-03	1.6395e-03

5.3. Flux distributions in two and three dimensions

We now investigate the impact of the source term on the flux distributions. The isotropic photon flux is defined by

$$q(\mathbf{x}) = \frac{1}{4\pi} \int_{S^2} u(\mathbf{x}, \hat{\omega}) d\sigma(\hat{\omega}).$$

For simplicity, vacuum boundary conditions are applied on all the boundaries. We always consider the isotropic scattering, and take $N = k = 2$ for the spatial discretization. The examples in this subsection are taken from the reference [33].

Example 5.4. *This problem is defined on a unit cube with vacuum boundaries. The first 0.2 by 0.2 by 0.2 region R contains a uniform isotropic source. For simplicity, we consider the following right-hand side function:*

$$f(\mathbf{x}, \boldsymbol{\omega}) = f(\mathbf{x}) = \begin{cases} 1, & \mathbf{x} \in R = [0, 0.2]^3, \\ 0, & \mathbf{x} \in D \setminus R. \end{cases}$$

The entire box is of uniform composition with the following data: $\sigma_t = 1$ and $\sigma_s = 0.4$.

For $z = 0.1$ fixed, the contour plot of the flux distributions with varying orders of the discrete ordinates is displayed in Fig. 5. We can see clearly that the contour map shows rays emanating from the source.

We now perform the test on the problem in (x, y) -geometry. In this case, all coefficients, the boundary data and the solution of (2.1)-(2.2) are independent of the space variable $x_3 = z$.

Example 5.5. *This problem is defined on a unit square with vacuum boundaries. The first 0.2 by 0.2 region localized in the lower left corner contains a uniform isotropic source. The entire box is of uniform composition with the following data: $\sigma_t = 1$ and $\sigma_s = 0.4$.*

For this example, we only consider the S_4 method. The contour plot of the flux distributions is displayed in Fig. 6 (a). Numerical results of other cases are listed in Fig. 6 (b)-(f) by changing the positions or increasing the numbers of the isotropic sources. In all cases, we again observe the rays emanating from the sources.

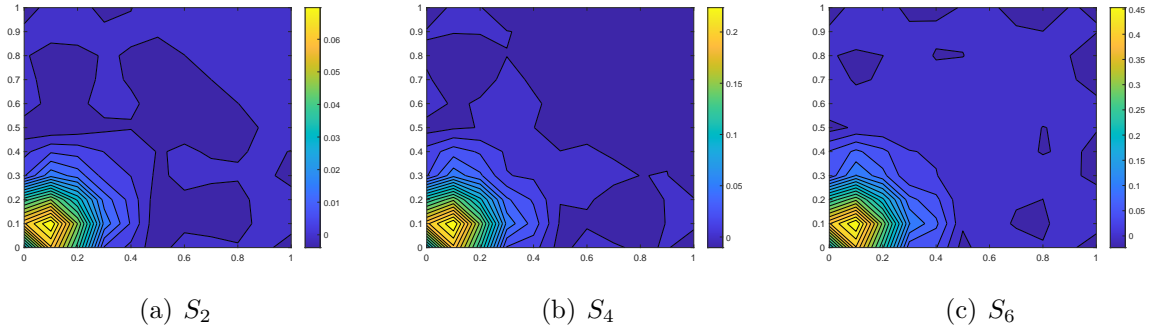


Fig. 5. Contour map of the photon flux distributions for Example 5.4

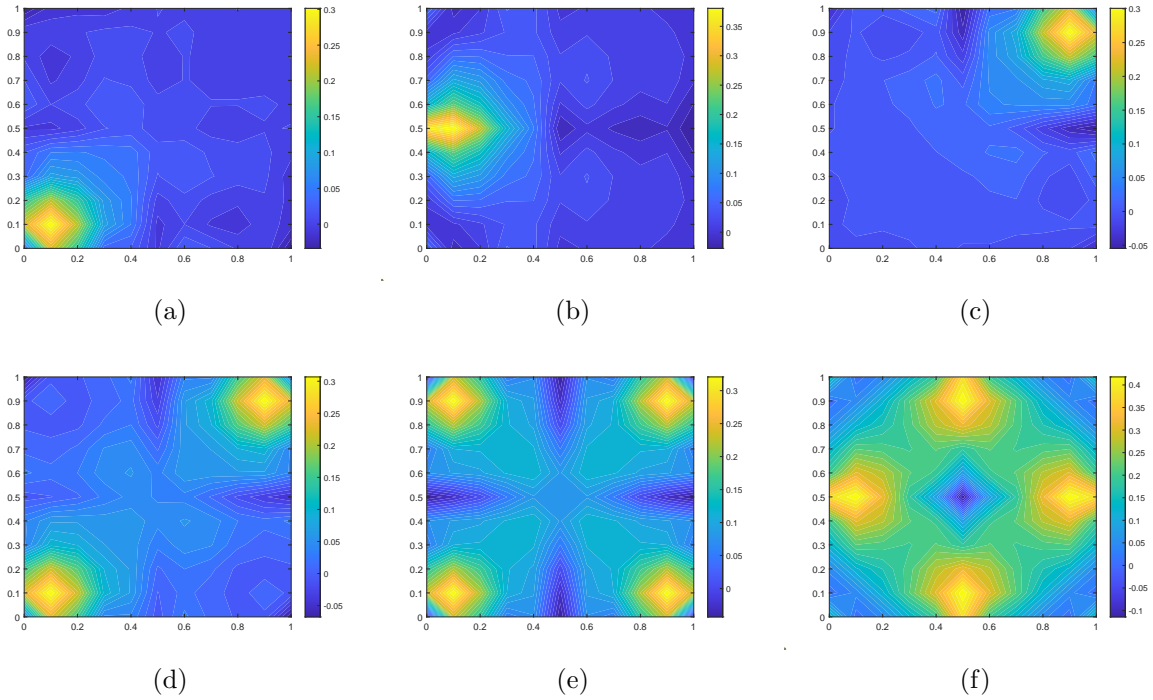


Fig. 6. Contour map of the photon flux distributions for Example 5.5

5.4. Examples with complex spatial domains in two dimensions

In the following, we extend the method to solve the RTE for some non-tensor product spatial domains in two dimensions. We always consider the isotropic scattering.

Example 5.6. The spatial domain D is an L-shaped region in 2-D displayed in Fig. 7, consisting of three rectangles R_1 , R_2 and R_2 , where

$$R_1 = \left\{ (x_1, x_2) : 0 \leq x_1 \leq 1, \quad 1 \leq x_2 \leq 2 \right\},$$

$$R_2 = \left\{ (x_1, x_2) : 0 \leq x_1 \leq 1, \quad 0 \leq x_2 \leq 1 \right\},$$

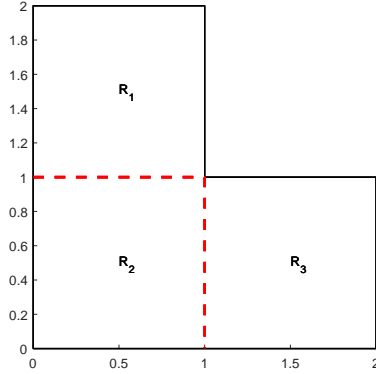


Fig. 7. Initial subdivision of a L -shaped region for Example 5.6

$$R_3 = \left\{ (x_1, x_2) : 1 \leq x_1 \leq 2, \quad 0 \leq x_2 \leq 1 \right\}.$$

The parameters are the same as Example 5.1 and the true solution is $u(\mathbf{x}, \boldsymbol{\omega}) = \sin(\pi x_1) \sin(\pi x_2)$.

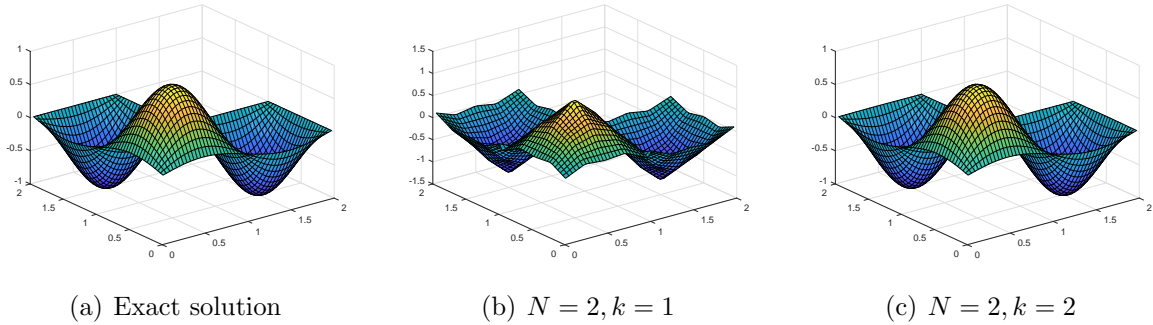


Fig. 8. Exact and numerical solutions for Example 5.6

Let $R = R_1 \cup R_2 \cup R_3$ be the initial subdivision of the L -shaped region and $\mathbf{V}_0^k(R)$ denote the piecewise polynomial space on R . We have the following orthogonal decomposition

$$\mathbf{V}_0^k(R) = \mathbf{V}_0^k(R_1) \oplus \mathbf{V}_0^k(R_2) \oplus \mathbf{V}_0^k(R_3),$$

where functions in $\mathbf{V}_0^k(R_j)$ ($j = 1, 2, 3$) are extended by zero to \mathbb{R}^2 . For each R_j , one can regard it as $[0, 1]^2$ and give the sparse representation by using an affine transformation. In Fig. 8, we display the numerical solutions for different N and k and the relative errors are given in Tab. 8.

Example 5.7. The spatial domain D is a circular region displayed in Fig. 9. The parameters and the true solution are the same as the last example.

Tab. 8. Relative errors for Example 5.6

N	$k = 1$	$k = 2$	$k = 3$	$k = 4$
1	2.2059e-01	1.6769e-02	1.7691e-03	1.3197e-04
2	6.1359e-02	2.1758e-03	1.1360e-04	4.1841e-06
3	1.7434e-02	3.0707e-04	7.2792e-06	2.1799e-07
4	4.8163e-03	4.2519e-05	4.6425e-07	-

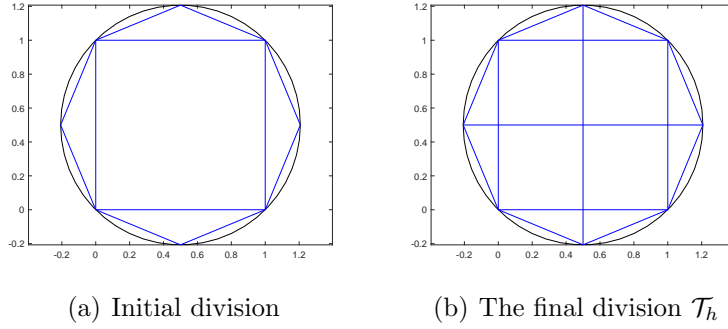


Fig. 9. Subdivision of the circular domain

To use the sparse grid method, we first plot a sufficiently large rectangle in the domain and approximate the boundary curve by a polygon as depicted in Fig. 9 (a). For simplicity, the boundary data corresponding to the polygon is obtained from the exact solution. For the general case, some approximation should be implemented, for example, the technique from the isoparametric finite elements. To avoid hanging nodes, the polygon approximation and the corresponding triangulation can be made consistent with the final partition of the rectangle, see Fig. 9 (b). We should note that the hanging nodes are allowed in our procedure since no interelement continuity is required. Denote the rectangle by R and the other triangles by T_1, \dots, T_8 , respectively. Let $\Omega = R \cup T_1 \cup \dots \cup T_8$. We then consider the initial DG space given by

$$\mathbf{V}_0^k(\Omega) = \mathbf{V}_0^k(R) \oplus \mathbf{V}_0^k(T_1) \oplus \dots \oplus \mathbf{V}_0^k(T_8).$$

The orthonormal bases corresponding to R has been given in the previous section, while the orthonormal bases on each T_i can be obtained by using the Gram-Schmidt procedure. For any triangle T with vertices $z_i = (x_i, y_i)$, $i = 1, 2, 3$, any point $z = (x, y)$ can be represented by the barycentric coordinates as

$$\begin{cases} x = x_1\lambda_1 + x_2\lambda_2 + x_3\lambda_3, \\ y = y_1\lambda_1 + y_2\lambda_2 + y_3\lambda_3, \\ 1 = \lambda_1 + \lambda_2 + \lambda_3. \end{cases}$$

Note that

$$\iint_T f(x, y)g(x, y)dx dy = 2|T| \int_0^1 \int_0^{1-\lambda_1} \tilde{f}(\lambda_1, \lambda_2)\tilde{g}(\lambda_1, \lambda_2)d\lambda_2 d\lambda_1,$$

Tab. 9. Orthonormal bases on the reference triangle τ for $k \leq 2$ ($r := \lambda_1, s := \lambda_2$)

$k = 0$	$\varphi_1 = \sqrt{2}$
$k = 1$	$\varphi_2 = 6r - 2$ $\varphi_3 = 2\sqrt{3}(2r + s - 1)$
$k = 2$	$\varphi_4 = \sqrt{6}(10r^2 - 8r + 1)$ $\varphi_5 = 3\sqrt{2}(5r - 1)(r + 2s - 1)$ $\varphi_6 = \sqrt{30}(r^2 + 6rs - 2r + 6s^2 - 6s + 1)$

where

$$\tilde{f}(\lambda_1, \lambda_2) := f(x(\lambda_1, \lambda_2), y(\lambda_1, \lambda_2)).$$

We then define an inner product on the reference triangle τ by

$$(\tilde{f}, \tilde{g})_\tau = \int_0^1 \int_0^{1-\lambda_1} \tilde{f}(\lambda_1, \lambda_2) \tilde{g}(\lambda_1, \lambda_2) d\lambda_2 d\lambda_1.$$

Given the orthonormal bases on τ by $\{\tilde{\varphi}_i\}$, we then obtain the bases on T given by

$$\psi_i(x, y) = \sqrt{\frac{1}{2|T|}} \varphi_i(x, y).$$

For any function $f(x, y)$ defined on T , the projection coefficients are computed as

$$\begin{aligned} c_i &= \iint_T f(x, y) \psi_i(x, y) dx dy = 2|T| \int_0^1 \int_0^{1-\lambda_1} \tilde{f}(\lambda_1, \lambda_2) \tilde{\psi}_i(\lambda_1, \lambda_2) d\lambda_2 d\lambda_1 \\ &= \sqrt{2|T|} \int_0^1 \int_0^{1-\lambda_1} \tilde{f}(\lambda_1, \lambda_2) \tilde{\varphi}_i(\lambda_1, \lambda_2) d\lambda_2 d\lambda_1 =: \sqrt{2|T|} \tilde{c}_i. \end{aligned}$$

The orthogonal bases on τ are obtained by using Gram-Schmidt procedure to the polynomial set $\{1, \lambda_1, \lambda_2, \lambda_1^2, \lambda_1 \lambda_2, \lambda_2^2, \dots\}$, some of which are listed in Tab. 9.

The relative error is defined by $\text{Err} = \|f - f_h\|_{L^2(\mathcal{T}_h)} / \|f\|_{L^2(\mathcal{T}_h)}$ and given in Tab. 10.

Tab. 10. Relative errors for Example 5.7 ($N = 2$)

k	0	1	2	3
Err	5.8510e-01	6.1678e-02	9.3273e-03	5.5965e-04

Summarizing our main observations from the numerical results reported in all previous examples, we may conclude that

- The sparse discrete ordinate DG method can greatly reduce the spatial degrees of freedom while keeping almost the same accuracy up to multiplication of an log factor.
- The proposed method is highly effective for problems away from strong forward scattering. To get an improved result, large discrete-ordinate sets are needed for highly forward-peaked case.
- The method can be extended to solve the RTE efficiently for some non-tensor product spatial domains in two dimensions.

6. Conclusions and remarks

In this paper, we combine the sparse grid technique with the discrete ordinate DG method to solve the RTE with inflow boundary conditions, which can be adapted to other types of boundary conditions. Under suitable regularity assumptions, we derive error estimates for the numerical solutions. Results from many numerical examples show the good convergence behavior of the method. For highly forward-peaked scattering, there have been substantial efforts made to develop simpler approximations to integral scattering operator S . One well-established example is the so-called Fokker-Planck equation (cf. [37]), to which the sparse grid techniques can also be applied.

Acknowledgments

The work was partially supported by NSFC (Grant No. 12071289) and the Strategic Priority Research Program of Chinese Academy of Sciences (Grant No. XDA25010402).

References

- [1] M. L. Adams and E. W. Larsen. Fast iteration methods for discrete-ordinates partial transport calculations. *Prog. Nucl. Energy*, 40(1):3–159, 2002.
- [2] V. Agoshkov. *Boundary Value Problems for Transport Equations*. Birkhauser, Boston, 1998.
- [3] B. Alpert. A class of bases in L^2 for the sparse representation of integral operators. *SIAM J. Math. Anal.*, 24(1):246–262, 1993.
- [4] B. Alpert, G. Beylkin, D. Gines, and L. Vozovoi. Adaptive solution of partial differential equations in multiwavelet bases. *J. Comput. Phys.*, 182:149–190, 2002.
- [5] M. Asadzadeh and A. Kadem. Chebyshev spectral- S_N method for the neutron transport equation. *Comput. Math. Appl.*, 52(3-4):509–524, 2006.
- [6] K. Atkinson and W. Han. *Spherical Harmonics and Approximations on the Unit Sphere: An Introduction*. Springer, Heidelberg, 2012.
- [7] D. Balsara. Fast and accurate discrete ordinates methods for multidimensional radiative transfer. Part I, basic methods. *J. Quant. Spectrosc. Radiat. Transf.*, 69(6):671–707, 2001.
- [8] S. C. Brenner and L. R. Scott. *The Mathematical Theory of Finite Element Methods*. Springer-Verlag, New York, 2008.
- [9] F. Brezzi, B. Cockburn, L. D. Marini, and E. Süli. Stabilization mechanisms in discontinuous galerkin finite element methods. *Comput. Methods Appl. Mech. Engrg.*, 195(25-28):3293–3310, 2006.
- [10] F. Brezzi, L. D. Marini, and E. Süli. Discontinuous Galerkin methods for first-order hyperbolic problems. *Math. Models Meth. Appl. Sci.*, 14(12):1893–1903, 2004.

- [11] R. E. Caflisch. Monte carlo and quasi-monte carlo methods. *Acta Numer.*, 7:1–49, 1998.
- [12] K. M. Case and P. F. Zweifel. *Linear Transport Theory*. Addison-Wesley, Reading, MA, 1967.
- [13] B. Chang, T. Manteuffel, S. McCormick, J. Ruge, and B. Sheehan. Spatial multigrid for isotropic neutron transport. *SIAM J. Sci. Comput.*, 29:1900–1917, 2007.
- [14] B. Cockburn. Discontinuous Galerkin methods. *ZAMM Z. Angew. Math. Mech.*, 83(11):731–754, 2003.
- [15] L. Dan, J. Cheng, and C. Shu. Conservative high order positivity-preserving discontinuous Galerkin methods for linear hyperbolic and radiative transfer equations. *J. Sci. Comput.*, 77(3):1801–1831, 2018.
- [16] J. J. Duderstadt and W. R. Martin. *Transport Theory*. John Wiley, New York, 1978.
- [17] P. Edström. A fast and stable solution method for the radiative transfer problem. *SIAM Rev.*, 47(3):447–468, 2005.
- [18] M. Frank, A. Klar, E. W. Larsen, and S. Yasuda. Time-dependent simplified P_N approximation to the equations of radiative transfer. *J. Comput. Phys.*, 226:2289–2305, 2007.
- [19] T. Gerstner and M. Griebel. Numerical integration using sparse grids. *Numer. Algorithms*, 18:209–232, 1998.
- [20] F. Golse, S. Jin, and C. Levermore. The convergence of numerical transfer schemes in diffusive regimes. I. Discrete-ordinate method. *SIAM J. Numer. Anal.*, 36(5):1333–1369, 1999.
- [21] K. Grella and C. Schwab. Sparse discrete ordinates method in radiative transfer. *Comput. Methods Appl. Math.*, 11(3):305–326, 2011.
- [22] M. Griebel. A parallelizable and vectorizable multi-level algorithm on sparse grids. Parallel algorithms for partial differential equations (kiel, 1990). *Notes Numer. Fluid Mech.*, 31:94–100, 1991.
- [23] M. Griebel. Adaptive sparse grid multilevel methods for elliptic PDEs based on finite differences. *Computing*, 61(2):151–179, 1998.
- [24] W. Guo and Y. Cheng. A sparse grid discontinuous Galerkin method for high-dimensional transport equations and its application to kinetic simulations. *SIAM J. Sci. Comput.*, 38(6):A3381–A3409, 2016.
- [25] W. Guo and Y. Cheng. An adaptive multiresolution discontinuous Galerkin method for time-dependent transport equations in multidimensions. *SIAM J. Sci. Comput.*, 39(6):A2962–A2992, 2017.
- [26] W. Han, J. Eichholz, and G. Wang. On a family of differential approximations of the radiative transfer equation. *J. Math. Chem.*, 50(4):689–702, 2012.
- [27] W. Han, J. Huang, and J. A. Eichholz. Discrete-ordinate discontinuous Galerkin methods for solving the radiative transfer equation. *SIAM J. Sci. Comput.*, 32(2):477–497, 2010.
- [28] A. D. Kim and M. Moscoso. Chebyshev spectral methods for radiative transfer. *SIAM J. Sci. Comput.*, 23:2074–2094, 2002.
- [29] M. Kindelan, F. Bernal, P. González-Rodríguez, and M. Moscoso. Application of the RBF meshless method to the solution of the radiative transport equation. *J. Comput. Phys.*, 229:1897–1908, 2010.
- [30] E. W. Larsen and J. E. Morel. *Advances in Discrete-ordinates Methodology*. Springer, New York, 2010.
- [31] E. E. Lewis and W. F. Miller. *Computational Methods of Neutron Transport*. John Wiley & Sons, New York, 1984.
- [32] P. Liu. A new phase function approximating to Mie scattering for radiative transport equations. *Phys. Med. Biol.*, 39:1025–1036, 1994.
- [33] J. A. Roberts. Direct solution of the discrete ordinates equations. 2010.
- [34] H. Sadat. On the use of a meshless method for solving radiative transfer with the discrete ordinates formulations. *J. Quant. Spectrosc. Radiat. Transf.*, 101:263–268, 2006.
- [35] C. Schwab, E. Süli, and R. A. Todor. Sparse finite element approximation of high-dimensional transport-dominated diffusion problems. *M2AN Math. Model. Numer. Anal.*, 42(5):777–819, 2008.
- [36] W. Shao, Q. Sheng, and C. Wang. A cascadic multigrid asymptotic-preserving discrete ordinate discontinuous streamline diffusion method for radiative transfer equations with diffusive scalings. *Comput. Math. Appl.*, 80(6):1650–1667, 2020.
- [37] Q. Sheng and W. Han. Well-posedness of the Fokker-Planck equation in a scattering process. *J. Math. Anal. Appl.*, 406(2):531–536, 2013.
- [38] Q. Sheng, C. Wang, and W. Han. An optimal cascadic multigrid method for the radiative transfer equation. *J. Comput. Appl. Math.*, 303:189–205, 2016.

- [39] S. A. Smoljak. Quadrature and interpolation formulae on tensor products of certain function classes. *Dokl. Akad. Nauk SSSR*, 148:1042–1045, 1963.
- [40] M. Tang. A uniform first-order method for the discrete ordinate transport equation with interfaces in X,Y-geometry. *J. Comput. Math.*, 27(6):764–786, 2009.
- [41] Z. Tao, Y. Jiang, and Y. Cheng. An adaptive high-order piecewise polynomial based sparse grid collocation method with applications. *arXiv:1912.03982v1*, pages 1–33, 2019.
- [42] C. Wang, H. Sadat, and J. Tan. First-order and second-order meshless formulations of the radiative transfer equation: a comparative study. *Numer. Heat Transfer B*, 66:21–42, 2014.
- [43] Z. Wang, Q. Tang, and W. Guo. Sparse grid discontinuous Galerkin methods for high-dimensional elliptic equations. *J. Comput. Phys.*, 314:244–263, 2016.
- [44] G. Widmer, R. Hiptmair, and C. Schwab. Sparse adaptive finite elements for radiative transfer. *J. Comput. Phys.*, 227(12):6071–6105, 2008.
- [45] D. Yuan, J. Cheng, and C. Shu. High order positivity-preserving discontinuous Galerkin methods for radiative transfer equations. *SIAM J. Sci. Comput.*, 38(5):A2987–A3019, 2016.
- [46] C. Zenger. Sparse grids. In W. Hackbusch, editor, Parallel algorithms for partial differential equations, Proceedings of the Sixth GAMM-Seminar, Kiel, 1990. *Notes on Num. Fluid Mech. Vieweg-Verlag*, 31:241–251, 1990.
- [47] M. Zhang, J. Cheng, and J. Qiu. High order positivity-preserving discontinuous galerkin schemes for radiative transfer equations on triangular meshes. *J. Comput. Phys.*, 397:108811, 2019.
- [48] H. Zheng and W. Han. On simplified spherical harmonics equations for the radiative transfer equation. *J. Math. Chem.*, 49(8):1785–1797, 2011.